Progress In Electromagnetics Research M, Vol. 107, 205–216, 2022

Investigation of On-Body Antenna Performance Using Motion Capture Technique and Statistical Analysis

George Lee[1], Daniel Agu[2, *], Brian Garner[3], and Yang Li[2]

Abstract—The field of wireless body area networks (WBANs) has seen growing interest in recent years due to applications of wearable devices, such as in healthcare. Effective on-body antenna design is necessary to provide optimal performance in real-world scenarios. This study compares several wearable antenna types, which are monopole, patch, and e-textile antennas, to determine how human body motion affects antenna performance using a human body phantom model and human volunteers. Monopole antenna overall outperforms the patch antenna at 915 MHz and the e-textile antenna at 2.45 GHz, and a Weibull distribution can be used as a probability distribution for S_{21} during an arm swing motion for all antenna types tested.

1. INTRODUCTION

On-body antenna analysis and design have received considerable interest in recent years due to the growing applications in wireless body area networks (WBANs). Several types of wearable antennas, such as monopole, microstrip, loop, planar inverted F antenna (PIFA), inverted F antenna (IFA), and patch array, have been implemented for on-body communication and sensing applications [1–10]. Researchers have compared the performance of these antennas when they are placed on the human body, and found that monopole antennas exhibit the best on-body transmission characteristics at ISM frequency bands. However, most comparative studies have only investigated cases where the human test subjects were standing still in a motionless position. For instance, in [2], the researchers compared horn-shaped self-complementary antennas (HSCAs) and planar inverted cone antennas (PICAs) attached to the head, chest, back, and arms of nonmoving human subjects and evaluated the root mean square delay spread and path loss performance of the antennas. In [7], a conventional coplanar waveguide antenna and tapered slot antennas were placed on the chest of a human subject, and their average fidelities were compared. In [8], monopole and loop antennas were compared in free space when they were placed in contact with a static human tissue model. Since human body movements can lead to considerable antenna characteristic changes such as impedance detuning and pattern distortion, and these changes may vary from one type of wearable antenna to another, it is desirable to investigate wearable antenna performance during experiments with humans in motion.

There are a limited number of studies comparing wearable antennas for dynamic motion scenarios. One study [11] shows that monopole-to-monopole on-body link exhibits higher transmission gain than links using patch and loop antennas during a walking scenario. Another study [12] compared various UHF 380–400 MHz dipole, PIFA, and PHARAD antennas, and showed that the PIFA had better communication coverage while the test subject walked in a campus environment. A third study [13] tested a patch antenna, inverted IFA, and circularly polarized microstrip antenna using waist-to-wrist, waist-to-chest, and waist-to-ankle channels at 2.45 GHz, showing that the patch antenna performed best

Received 2 December 2021, Accepted 17 January 2022, Scheduled 25 January 2022
* Corresponding author: Daniel Ugochukwu Agu (daniel_agu@baylor.edu).
[1] Department of Biomedical Engineering, Rensselaer Polytechnic Institute, New York, USA. [2] Department of Electrical and Computer Engineering, Baylor University, Texas, USA. [3] Department of Mechanical Engineering, Baylor University, Texas USA.

based on shadowing. While these studies [11–13] have compared antenna effects with the human body moving, they did not quantify the relationship between motion patterns and transmission links between on-body antennas. Since human body motion can introduce as much as 30 dB fluctuation in on-body transmission gain [14], pinpointing which wearable antenna performs best and at what body position will provide great insights into on-body antenna design and channel analysis.

In this study, we utilize motion-capture technology to record human body motions during different on-body antenna transmission scenarios. We have previously used similar techniques to study on-body monopole antenna performance [14], and we here extend this work to include three commonly-used wearable antennas: monopole, microstrip, and e-textile antennas. Furthermore, in addition to human subjects, we herein also utilize an in-house human phantom model with arm swinging capability to create a controlled environment for the collection of on-body antenna transmission data. Combining motion-capture analysis with a human phantom model provides a unique and powerful way to evaluate the performance of different types of on-body antennas during dynamic experiments. Lastly, a statistical analysis is performed to identify the optimum distribution fit for multiple antenna types, antenna configurations, and test subjects.

This paper is organized as follows. Section 2 presents the on-body antennas used in this study, the setup of the motion capture system and human phantom model, and the methods for collecting antenna transmission data. Section 3 shows the measurement results, and compares and discusses the performances of different types of on-body antennas. Section 4 displays the optimum distribution fit for the on-body transmission links of different antenna types from a statistical analysis.

2. MATERIALS & METHODS

The four antenna pairs used in this study are two monopole pairs resonating at 915 MHz and 2.45 GHz, respectively, one microstrip pair at 915 MHz, and e-textile pair at 2.45 GHz. The 915 MHz and 2.45 GHz operating frequencies were selected because they are located in the ISM frequency band and are commonly used for wearable applications. Samples of the antennas used in this study can be seen in Fig. 1. The quarter wavelength monopole antennas consist of a steel bridge ground plane and 18-gage copper wire that is 82 mm long for the 915 MHz and 30.5 mm long for the 2.45 GHz. The microstrip patch antenna is fabricated with an FR-4 substrate and copper, with a patch size of 97.68 mm by 76.53 mm. The e-textile antenna is fabricated using machine embroidery with the fabric dipole having a length of 24 mm for each arm, a 5 mm bend, and a 2 mm width. All three antenna types utilize a coaxial feed.

(a) (b) (c)

Figure 1. (a) 915 MHz monopole antenna. (b) 915 MHz microstrip patch antenna. (c) 2.45 GHz e-textile antenna.

We included two human subjects and a human phantom model to test antenna performance. Fig. 2 shows the phantom model (a) and one of the human volunteers (b), each having one microstrip patch antenna placed on the chest and the other placed on the left wrist. The setup as shown in Fig. 2 is conducted in a large, open space with the ground being the only source of significant reflections, and multiple absorbers are placed on the ground to minimize such reflections. Table 1 shows the

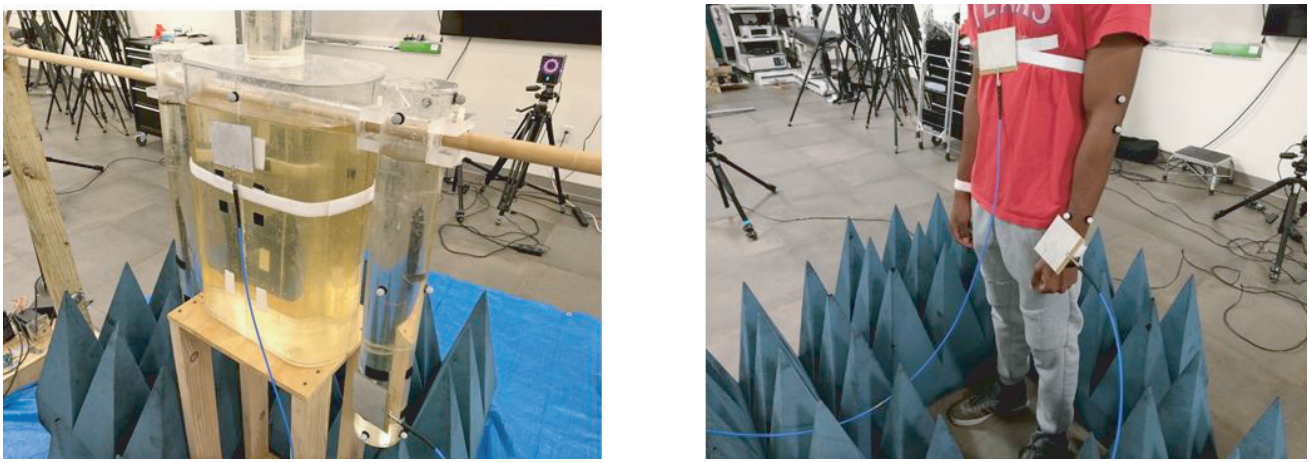

(a) (b)

Figure 2. (a) Human upper body phantom model, and (b) human volunteer.

Table 1. Phantom model and human volunteer dimensions.

Subject	Torso Circumference (cm)	Torso Length (cm)	Arm Circumference (cm)	Arm Length (cm)
Phantom Model	102.9	53.7	33	68.6
Human Volunteer A	111.8	54	30.6	57.5
Human Volunteer B	103.5	50	29.5	56.5

Table 2. Dielectric properties of the phantom model muscle tissue mimicking solution.

	915 MHz	2.45 GHz
Muscle Tissue Relative Permittivity (Measured)	54.45	36.28
Muscle Tissue Relative Permittivity (Theoretical)	55.9	59.98
Conductivity (S/m) (Measured)	1.14	2.75
Conductivity (S/m) (Theoretical)	0.97	2.17

key dimensions of the phantom model and of the human volunteers. The phantom model is a hollow plexiglass design filled with dielectric solutions that allow for modifying the dielectric properties of the phantom to match those of human muscle tissue. For this study the solution mimicking muscle tissue consists of 53.0% distilled water, 48.5% sugar, and 1.2% salt by mass, which is based on values from [15]. The relative permittivity and conductivity of the solution have been measured using a dielectric probe and are presented in Table 2. It is shown that the permittivity of the solution is close to that of human muscle at 915 MHz and close to 2/3 that of human muscle at 2.45 GHz [16]. Both values have been shown to effectively model the human body [14].

This study uses a measurement technique that involves simultaneous, time-synchronized collection of antenna transmission data and motion capture data. The antenna transmission data (S_{21}) are collected using an Agilent N5230C PNA-L vector network analyzer (VNA). The motion capture data

are collected using a Vicon motion capture system consisting of Vantage 5 and 8 model cameras, and a Phasespace Impulse motion capture system. The motion capture system and the VNA are time synchronized using the VNA's external trigger mechanism, allowing both to begin collecting data simultaneously at a rate of 120 Hz.

During a given data collection trial either the phantom model or one of the human volunteers performs repeated cycles swinging the left arm at the shoulder forwards and backwards in the sagittal plane at a rate of one cycle every 3.0 s. One cycle of arm swinging is defined as the arm starting at its furthest point of shoulder flexion in front of the body (chest side), extending the shoulder to the furthest point behind the body, then flexing again to the furthest point in front of the body. The furthest point in each direction is based on the calculation of the arm angle using motion capture data. The arm angle refers to the angle created between the arm and torso when being viewed from the sagittal plane, which results in a 0° angle when the arm is at the side of the body, a positive arm angle when the arm is in front (anterior) of the torso, and a negative arm angle when the arm is behind (posterior) the torso. The largest magnitude positive arm angle indicates the time when the arm is at its furthest in front of the body, and the largest magnitude negative arm angle indicates the time when the arm is at its furthest behind the body. The swinging arm is kept straight with the elbow fully extended and palm facing medially toward the body. Motion capture markers are placed on the left arm of the phantom and human volunteers to allow data recording of the arm swinging motion. The motion capture markers, which can be seen in Fig. 2(b), are placed, so the arm, which is held straight during the swinging motion, can be approximated as a line, allowing for arm angle to be found using the markers on the arm.

The antennas are placed for different trials in one of three configurations: chest/left wrist (front), chest/left wrist (back), and both wrists (front). Wrist (front) denotes an antenna placed on the radial (thumb) side of the wrist which faces forward during the arm swinging motion, and wrist (back) denotes an antenna placed on the ulnar side of the wrist which faces backward during the arm swinging motion. Although this study focuses only on wearable antennas located on chest and wrist, it establishes a methodology and measurement platform that can be extended to other locations of the body. Fig. 1 shows the phantom model and human volunteer wearing microstrip antennas in the chest/left wrist (front) antenna configuration. During each arm-swinging motion trial, the motion capture and antenna transmission data (S_{21}) are recorded simultaneously for 20 s. We note that there were also variations in the reflection coefficient data (S_{11}) due to body movements, but S_{11} were consistently below -10 dB at the frequencies of interest for the entire duration of the experimental trials, implying that the antennas always had good impedance match. Furthermore, there would also be variations in the radiation pattern, which is included in the S_{21} measurement results. Three trials are performed by each of the three participants (phantom and two human volunteers), for each of the four antenna pairs, and for each of the three antenna configurations, resulting in a total of one hundred and eight ($3*3*4*3$) experimental trials performed.

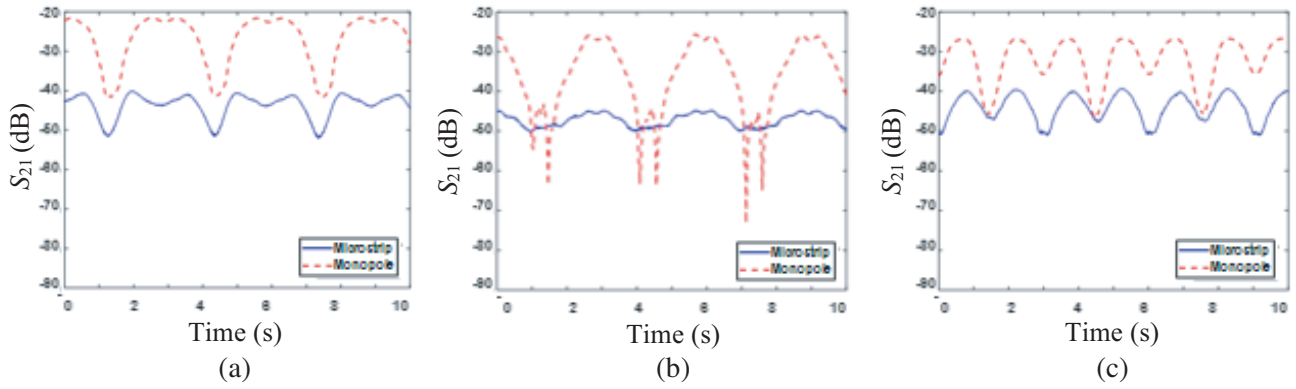

Figure 3. S_{21} signal magnitude vs time for the phantom model wearing 915 MHz microstrip (solid blue) and 915 MHz monopole (dashed red) antennas in the (a) chest/left wrist (front), (b) chest/left wrist (back), and (c) both wrists (front) antenna configurations.

3. RESULTS

3.1. 915 MHz: Microstrip vs. Monopole

In Fig. 3, the antenna transmission coefficients collected on the phantom model are plotted for both the 915 MHz microstrip and 915 MHz monopole antenna pairs for each of the three antenna placement configurations. Fig. 3(a) shows that with the chest/left wrist (front) configuration, both types of antennas exhibit M-shaped, periodic fluctuation patterns which match the 3.0 second arm swing cycle of the phantom model. The monopole antenna shows superior performance over the microstrip antenna, with an average S_{21} of 18.93 dB higher in the transmission coefficient over the 10 second window.

Similar observations can be made for the other two placement configurations, as shown in Figs. 3(b) and (c). The monopole antenna has much better S_{21} gain than the microstrip antenna for most all phantom arm positions, with the monopole having a higher average S_{21} of 12.79 dB for the chest/left wrist (back) configuration and 12.23 dB for the both wrists (front) configuration. Again, the monopole antenna exhibits more signal magnitude fluctuation than the microstrip antenna.

Analyzing how the S_{21} gain varies with arm swing angle can provide additional insights into the effect of body position and motion on transmission coefficients. Fig. 4 shows S_{21} vs arm angle for the phantom model comparing 915 MHz microstrip and 915 MHz monopole antennas. Fig. 4(a) for the chest/left wrist (front) antenna configuration shows that S_{21} is overall higher at positive arm flexion angles (arm in front of the body) and lower at negative arm angles (arm behind the body) for both antennas, suggesting that S_{21} is higher when there exists a line-of-sight path between the transmitting and receiving antennas. The chest/left wrist (back) antenna configuration also shows, in Fig. 4(b), a higher S_{21} at positive arm angles for both the microstrip and monopole antennas. In contrast, the both wrists (front) antenna configuration shows in Fig. 4(c) that the lowest S_{21} occurs at positive arm angles, and the highest S_{21} appears around zero degrees for both types of antennas.

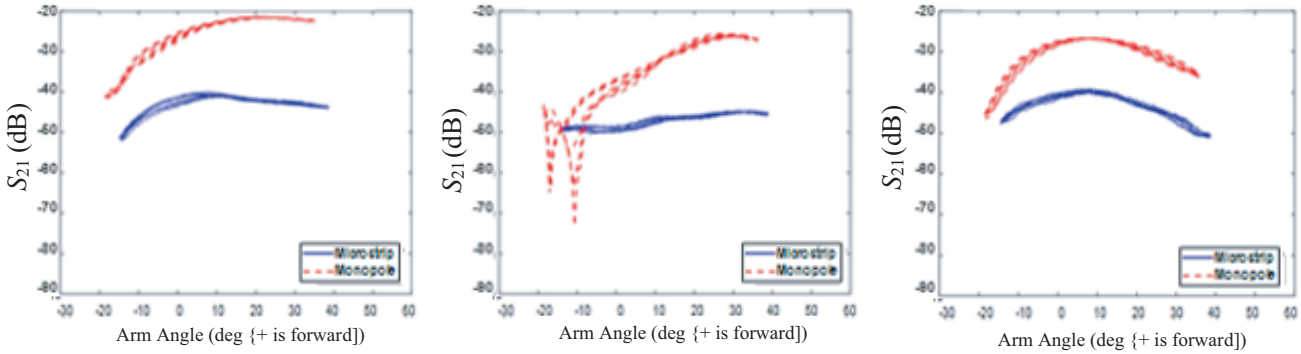

Figure 4. S_{21} vs arm angle for the phantom model wearing 915 MHz microstrip and 915 MHz monopole antennas in the (a) chest/left wrist (front), (b) chest/left wrist (back), and (c) both wrists (front) antenna configurations.

To verify the above results from the phantom experiments, we conducted similar measurements with human test subjects. Figs. 5 and 6 show the S_{21} gain versus time and versus arm swing angles, respectively, for human volunteer A wearing 915 MHz microstrip and 915 MHz monopole antennas for comparison. Unlike the phantom model data sets, there is less consistency in the periodicity of the arm swings of the human volunteer despite the use of a metronome to assist in keeping a 3.0 s arm swing cycle. Although the arm swing cycles do not directly align in time, all three antenna configurations show similar peak and dip patterns for both the microstrip and monopole, as with the phantom measurements. The monopole antenna again exhibits better gain and larger signal fluctuations. Both microstrip and monopole antenna types exhibit reduced gain at negative arm angles (arm extension behind the body), except for the microstrip antenna for the both wrists (front) configuration (Fig. 6(c), blue solid line).

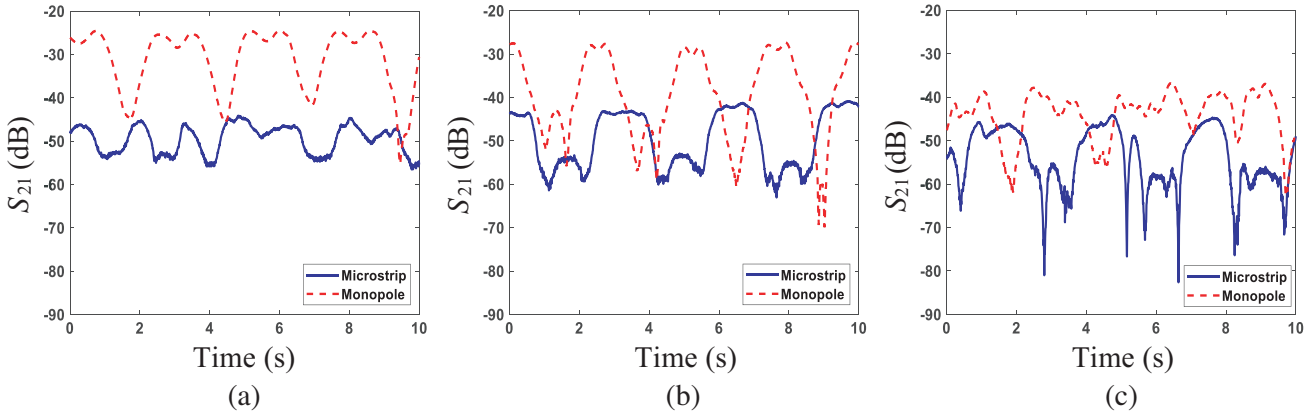

Figure 5. S_{21} vs time for human volunteer A wearing 915 MHz microstrip and 915 MHz monopole antennas in the (a) chest/left wrist (front), (b) chest/left wrist (back), and (c) both wrists (front) antenna configurations.

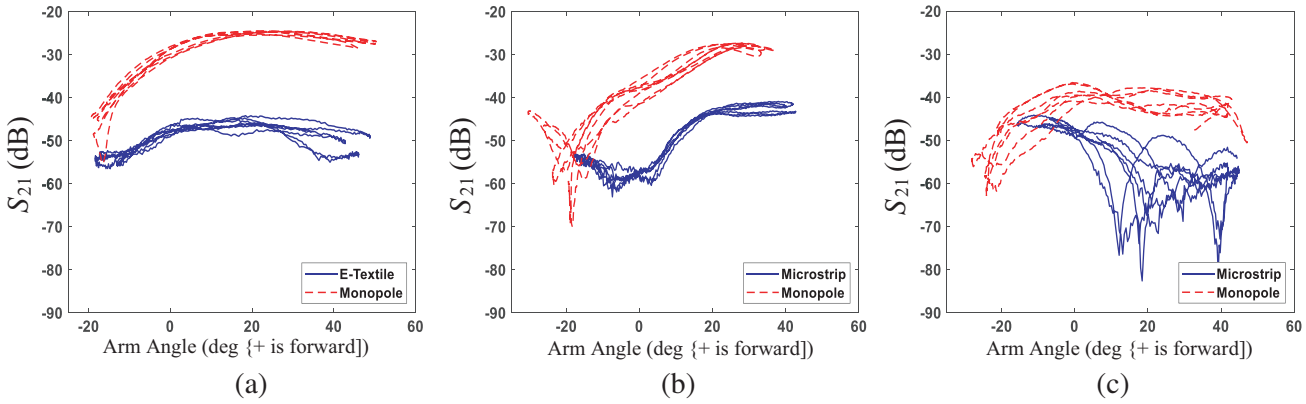

Figure 6. S_{21} vs arm angle for human volunteer A wearing 915 MHz microstrip and 915 MHz monopole antennas in the (a) chest/left wrist (front), (b) chest/left wrist (back), and (c) both wrists (front) antenna configuration.

3.2. 2.45 GHz: E-Textile Dipole vs. Monopole

Figure 7 shows S_{21} vs time for the phantom model comparing the 2.45 GHz e-textile dipole antennas and monopole antennas. While the transmission data between monopole antennas are much higher than that of the e-textile dipoles for the chest/left wrist (front) antenna configuration (Fig. 7(a)), the two types of antennas have similar performance for the both wrists (front) configuration (Fig. 7(c)). The difference in average S_{21} for the chest/left wrist (front) configuration is 24.69 dB, compared to the difference in average S_{21} for the both wrists (front) configuration of 0.30 dB. The difference in average S_{21} for the chest/left wrist (back) (Fig. 7(b)) falls between the chest/left wrist (front) and both wrists (front) configurations with a value of 14.79 dB. The peak transmission coefficients are more consistent across antenna configurations for the e-textile dipole than the monopole, suggesting that the performance of different antenna types will have different sensitivities to antenna placement.

Figure 8 shows S_{21} vs arm angle for the phantom model comparing the 2.45 GHz e-textile antennas and monopole antennas. As seen at 915 MHz, the monopole S_{21} gain pattern at 2.45 GHz is relatively smooth over the arm angle range of motion, but is less so for the both wrists (front) antenna configuration. However, the e-textile antenna exhibits sharp drops in S_{21} gain at specific arm angle positions, and the angle locations where these drops occur somewhat depend on the antenna placement configuration. For the both wrists (front) antenna configuration, an S_{21} dip occurs at -10 deg, and a

secondary S_{21} dip occurs around positive 32 deg. Similar dips occur around −5 deg and 12 deg for the other antenna placement configurations. Again for 2.45 GHz, the chest/left wrist (front) and chest/left wrist (back) antenna configurations exhibit the lowest S_{21} values at negative arm angles, and S_{21} is generally higher at positive arm angles.

The same measurements and comparisons were repeated on a real human test subject. Figs. 9 and 10 show S_{21} versus time and versus arm angle for human volunteer B comparing the 2.45 GHz e-textile antennas and monopole antennas. The measurement data collected with the human subjects confirm the advantage of the monopole over the e-textile dipole for the chest/left wrist (front) and chest/left wrist (back) antenna configurations, but the difference between the two types of antennas is smaller for the both wrists (front) configuration.

4. DISCUSSION

The advantage of the monopole over the microstrip antenna shown in Figs. 3–6 and the e-textile antenna shown in Figs. 7–10 can be attributed to different radiation patterns and the excitation of on-body creeping waves. It is also evident that the S_{21} signal magnitude fluctuates more (e.g., peak-to-bottom difference) for the monopole antenna than for the microstrip patch, seen in Figs. 3 and 4, implying a higher sensitivity to arm position over the cycle of swinging motion for the monopole than the microstrip.

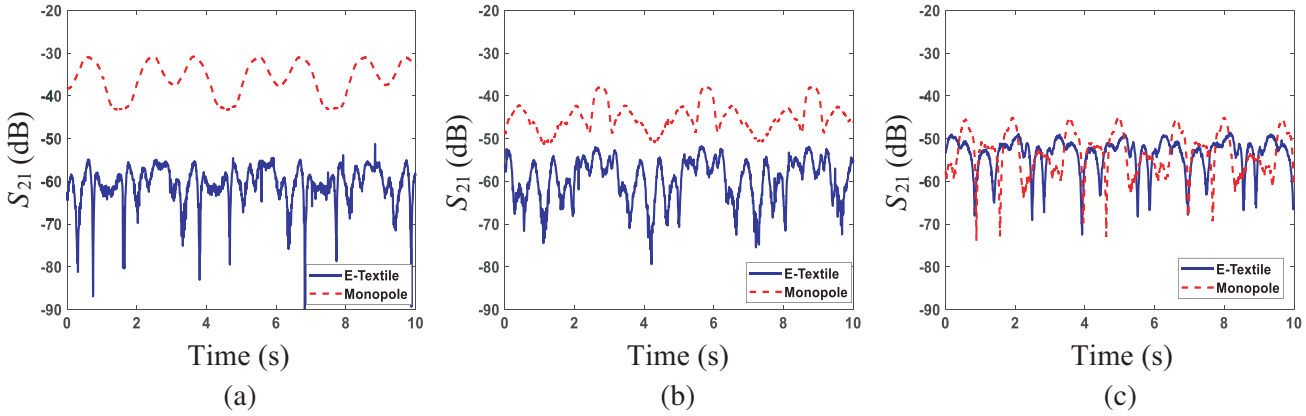

Figure 7. S_{21} vs time for the phantom model wearing 2.45 GHz e-textile and 2.45 GHz monopole antennas in the (a) chest/left wrist (front), (b) chest/left wrist (back), and (c) both wrists (front) antenna configurations.

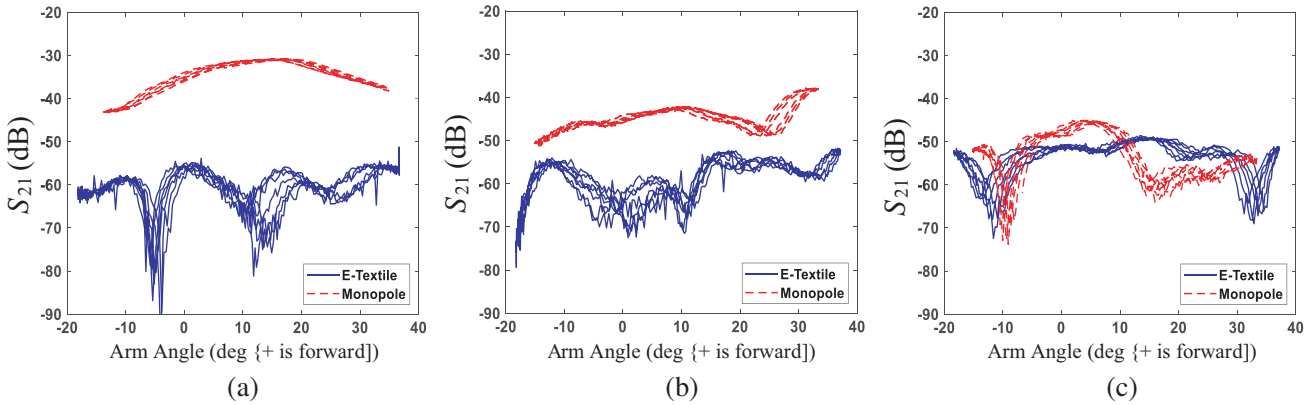

Figure 8. S_{21} vs arm angle for the phantom model wearing 2.45 GHz e-textile and 2.45 GHz monopole antennas in the (a) chest/left wrist (front), (b) chest/left wrist (back), and (c) both wrists (front) antenna configurations.

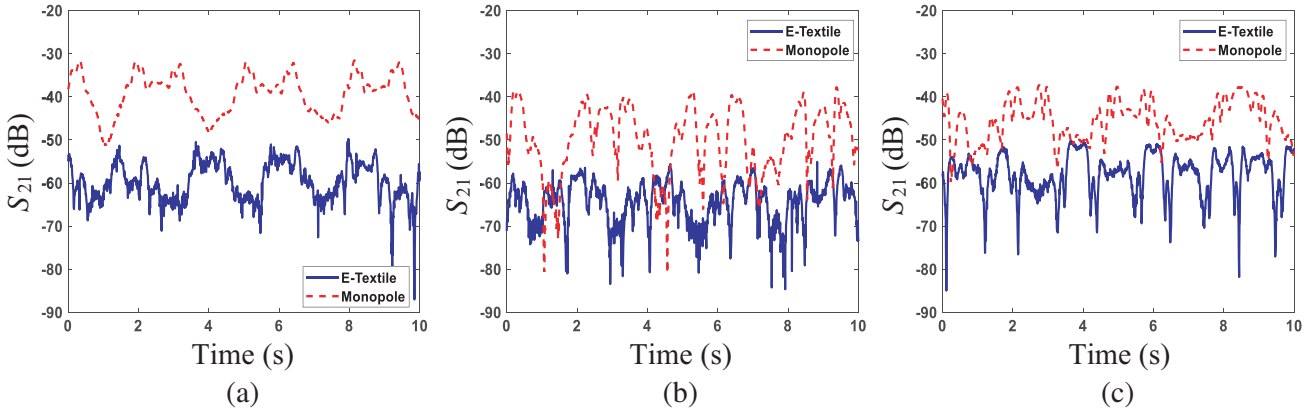

Figure 9. S_{21} vs time for human volunteer B wearing 2.45 GHz e-textile and 2.45 GHz monopole antennas in the (a) chest/left wrist (front), (b) chest/left wrist (back), and (c) both wrists (front) antenna configurations.

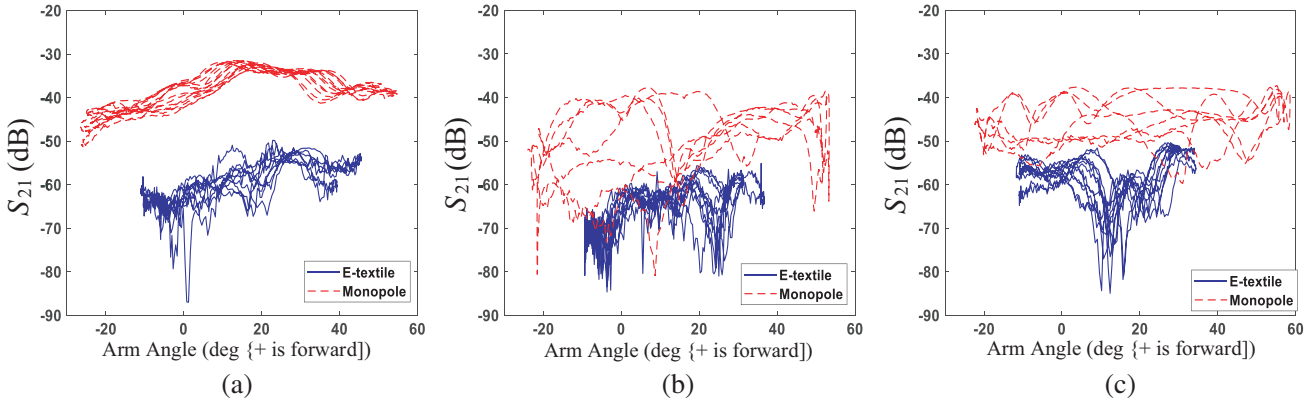

Figure 10. S_{21} vs arm angle for human volunteer B wearing 2.45 GHz e-textile and 2.45 GHz monopole antennas in the (a) chest/left wrist (front), (b) chest/left wrist (back), and (c) both wrists (front) antenna configuration.

Although the human data show similar patterns and magnitude trends to the phantom data, the human data show less consistency per arm swing due to the arm range of motion being less controllable with the human subjects, which is most noticeable in the e-textile antenna data, shown in Figs. 7–10.

Statistical analysis of the time-varying transmission data provides a quantitative analysis and additional insight into on-body antenna performance. Previous studies have employed various probability density functions (PDFs), such as normal [4, 17], lognormal [5, 17, 18], Nakagami [17, 18], Rice [18, 19], shadowed κ-μ [18, 20], Gamma [17], Rayleigh [17], and Weibull [17], to analyze path loss and linear fading envelope. Various methods of quantifying distribution fit include correlation coefficient [20] and Chi-square testing [4]. However, most of the previous efforts were not directly applied to on-body antenna transmission scenarios. In this work, we utilize the Weibull PDF distribution to fit our measured phantom and real human data since it shows overall better fits through comparison of different antenna types and antenna configurations. The goodness of the fit is evaluated using the sum of squared estimate of errors (SSE).

The Weibull PDF can be represented by the following equation:

$$f(x|a,b) = \frac{b}{a}\left(\frac{x}{a}\right)^{b-1} e^{-\left(\frac{x}{a}\right)^{b}} \tag{1}$$

where a is the scale factor and b is the shape factor.

The fit of the Weibull distribution PDF is evaluated using the sum of squared estimate of errors

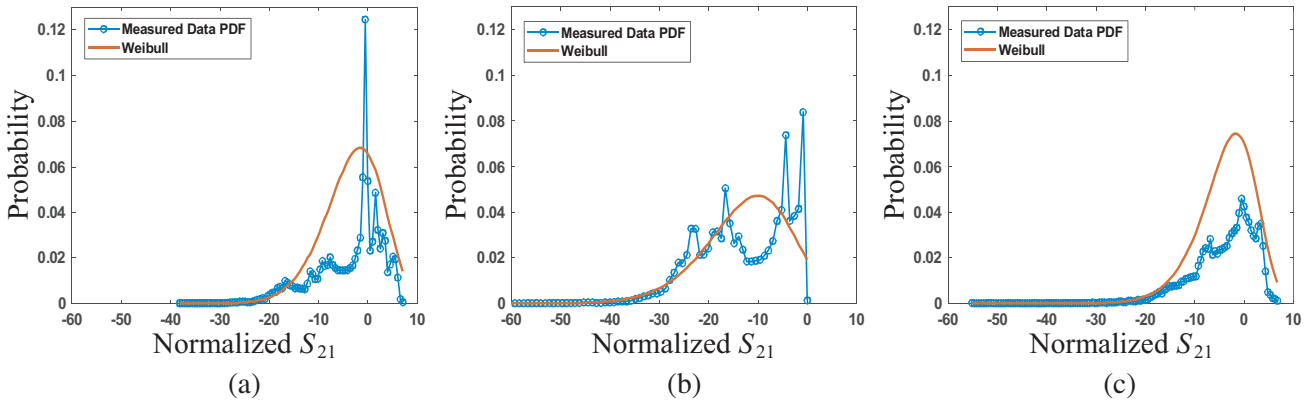

Figure 11. PDF of measured S_{21} values and fitted Weibull PDF for combined phantom and human volunteer data sets with the 915 MHz monopole antennas for the (a) chest/left wrist (front), (b) chest/left wrist (back), and (c) both wrists (front) antenna configurations.

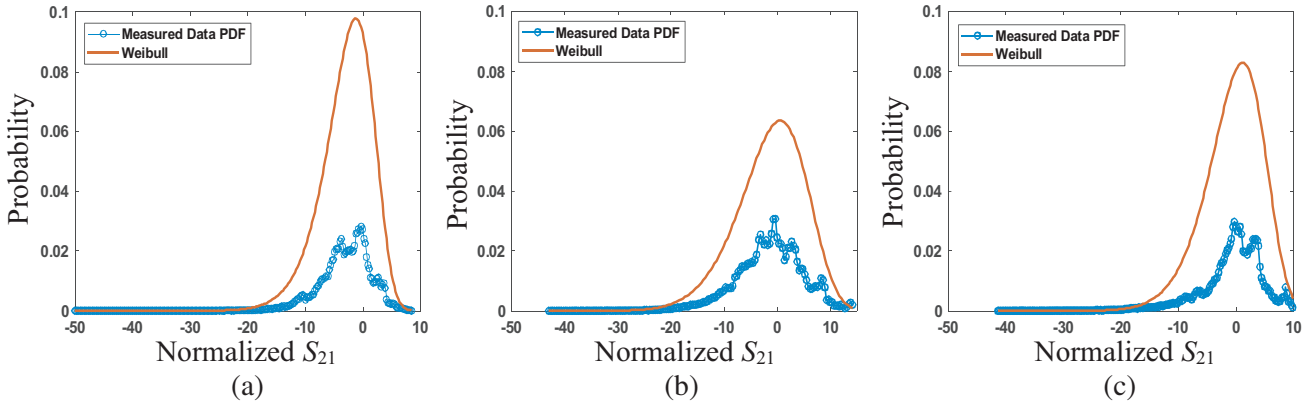

Figure 12. PDF of measured S_{21} values and fitted Weibull PDF for combined phantom and human volunteer data sets with the 915 MHz microstrip antennas for the (a) chest/left wrist (front), (b) chest/left wrist (back), and (c) both wrists (front) antenna configurations.

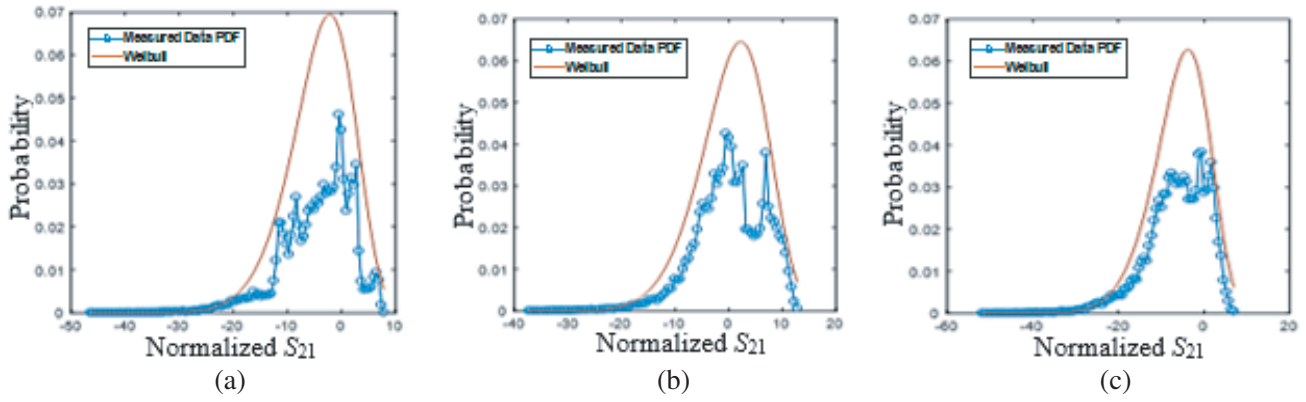

Figure 13. PDF of measured S_{21} values and fitted Weibull PDF for combined phantom and human volunteer data sets with the 2.45 GHz monopole antennas for the (a) chest/left wrist (front), (b) chest/left wrist (back), and (c) both wrists (front) antenna configurations.

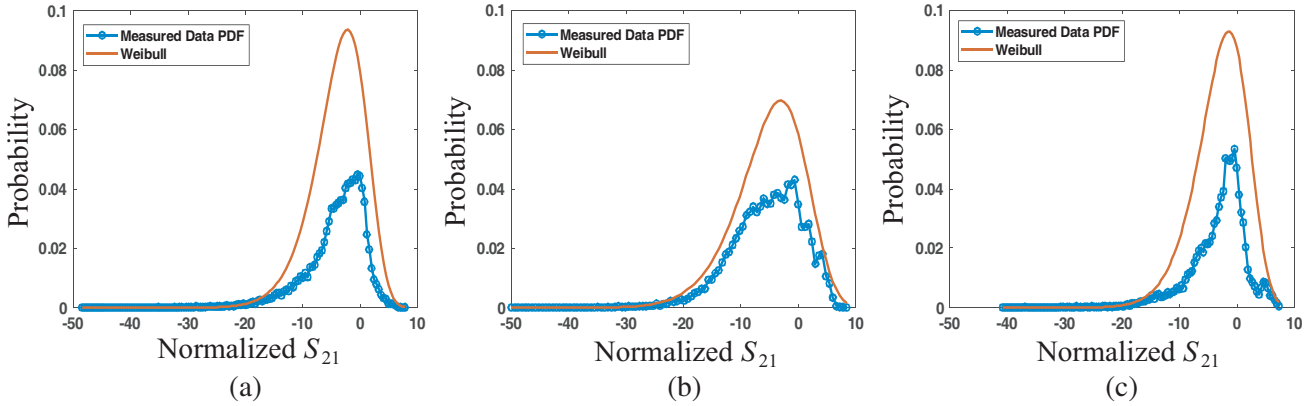

Figure 14. PDF of measured S_{21} values and fitted Weibull PDF for combined phantom and human volunteer data sets with the 2.45 GHz e-textile antennas for the (a) chest/left wrist (front), (b) chest/left wrist (back), and (c) both wrists (front) antenna configurations.

Table 3. Weibull distribution characteristics and fit for on-body antennas.

Antenna and Antenna Configuration	Weibull, a value	Weibull, b value	SSE	Mean (dB)	Standard Deviation (dB)
915 MHz Monopole, Chest/Left Wrist (front)	37.43	6.87	0.0351	−22.47	12.41
915 MHz Monopole, Chest/Left Wrist (back)	53.15	6.72	0.0119	−34.78	6.20
915 MHz Monopole, Both Wrists (front)	53.97	10.86	0.0297	−40.01	8.91
915 MHz Microstrip, Chest/Left Wrist (front)	52.78	13.98	0.1725	−43.45	13.62
915 MHz Microstrip, Chest/Left Wrist (back)	44.34	7.58	0.0544	−44.56	14.10
915 MHz Microstrip, Both Wrists (front)	43.02	9.57	0.1279	−46.23	15.00
2.45 GHz Monopole, chest/left wrist (front)	44.87	8.41	0.0318	−38.75	6.62
2.45 GHz Monopole, chest/left wrist (back)	40.35	7.01	0.02	−47.52	6.59
2.45 GHz Monopole, both wrists (front)	48.69	8.25	0.01	−50.97	7.44
2.45 GHz E-textile, Chest/Left Wrist (front)	46.56	11.80	0.0532	−60.64	5.13
2.45 GHz E-textile, Chest/Left Wrist (back)	51.66	9.72	0.0136	−57.74	5.60
2.45 GHz E-textile, Both Wrists (front)	39.76	9.99	0.0612	−61.93	6.60

(SSE), which is calculated using the following equation:

$$SSE = \sum_{i=1}^{n} \left(y_i - f\left(x_i\right)\right)^2 \tag{2}$$

The PDF of the measured data and a Weibull PDF fit of the measured data using combined phantom and human volunteer data sets are provided in Fig. 11 for the 915 MHz monopole antennas, Fig. 12 for the 915 MHz microstrip antennas, Fig. 13 for the 2.45 GHz monopole antennas, and Fig. 14 for the 2.45 GHz e-textile antennas. The Weibull distribution a value, b value, and SSE are shown in Table 3. The minimum SSE values indicate that the Weibull distribution is able to show good agreement with the PDF of the measured S_{21} data sets for all three antenna types.

5. CONCLUSION

Antenna signal data and motion capture data were recorded synchronously during a series of experimental trials involving two human volunteers and a human phantom model performing single arm swing activities with trial variations including three antenna types (Monopole, microstrip, and e-textile), two antenna frequencies (915 MHz, 2.45 GHz), and three antenna placement configurations. Comparisons of S_{21} transmission are presented versus time and versus arm swing angle across the different antenna types, placement configurations, and frequencies. The phantom model continues to prove an effective, convenient, and well-controlled representative for studying human on-body EM wave propagation, especially for on-body antenna applications. The results showed that overall the monopole antenna showed better S_{21} transmission performance than the microstrip at 915 MHz and e-textile at 2.45 GHz. The monopole also demonstrated less sensitivity to antenna placement. A statistical analysis of S_{21} showed that a Weibull PDF has good agreement with measured S_{21} values, which provides a valuable tool for determining the probability of S_{21} falling below a given threshold value for quantifying antenna on-body antenna performance for motion scenarios.

Future planned work includes expanding the study to additional antenna types, body motions, and antenna placements. Additionally, the phantom model can be used to optimize antenna designs to perform better during on-body scenarios.

REFERENCES

1. Kamarudin, M. R., Y. I. Nechayev, and P. S. Hall, "Performance of antennas in the on-body environment," *2005 IEEE Antennas and Propagation Society International Symposium*, July 2005.
2. Alomainy, A., Y. Hao, C. G. Parini, and P. S. Hall, "Comparison between two different antennas for UWB on-body propagation measurements," *IEEE Antennas and Wireless Propagation Letters*, Vol. 4, 31–34, 2005.
3. Ghannoum, H., C. Roblin, and S. Bories, "UWB antennas in body area networks," *IEEE International Workshop on Antenna Technology Small Antennas and Novel Metamaterials*, March 2006.
4. Hao, Y., A. Alomainy, Y. Zhao, C. G. Parini, Y. Nechayev, P. Hall, and C. C. Constantinou, "Statistical and deterministic modelling of radio propagation channels in WBAN at 2.45 GHz," *2006 IEEE Antennas and Propagation Society International Symposium*, July 2006.
5. Alomainy, A., Y. Hao, A. Owadally, C. G. Parini, Y. Nechayev, C. C. Constantinou, and P. S. Hall, "Statistical analysis and performance evaluation for on-body radio propagation with microstrip patch antennas," *IEEE Transactions on Antennas and Propagation*, Vol. 55, No. 1, 245–248, January 2007.
6. Alomainy, A., A. Sani, A. Rahman, J. G. Santas, and Y. Hao, "Transient characteristics of wearable antennas and radio propagation channels for ultrawideband body-centric wireless communications," *IEEE Transactions on Antennas and Propagation*, Vol. 57, No. 4, 875–884, April 2009.
7. Koohestani, M., A. A. Moreira, and A. K. Skrivervik, "System fidelity factor evaluation of wearable ultra-wideband antennas for on-body communications," *IET Microwaves, Antennas, and Propagation*, Vol. 9, No. 10, 1054–1058, July 2015.

8. Touvinen, T., K. Y. Yazdandoost, and J. Iinatti, "Comparison of the performance of the two different UWB antennas for the use in WBAN on-body communications," *2012 6th European Conference on Antennas and Propagation (EUCAP)*, March 2012.
9. Hall, P. and Y. Hao, *Antennas and Propagation for Body-Centric Wireless Communications*, 2nd Edition, Ch. 3, 63–106, Artech House, Norwood, MA, USA, 2012.
10. Conway, G. and W. Scanlon, "Antennas for over-body-surface communication at 2.45 GHz," *IEEE Transactions on Antennas and Propagation*, Vol. 57, No. 4, 884–855, April 2009.
11. Touvinen, T., K. Y. Yazdandoost, and J. Iinatti, "Comparison of the performance of the two different UWB antennas for the use in WBAN on-body communications," *2012 6th European Conference on Antennas and Propagation (EUCAP)*, March 2012.
12. Trajkovkj, J., J. Zürcher, and A. Skrivervik, "Performance of UHF W-BAN antennas in a real environment scenario," *2014 Loughborough Antennas and Propagation Conference (LAPC)*, November 2014.
13. Paraskevopoulos, A., A. Alexandridis, T. Zervos, A. Michalopoulou, F. Lazarakis, and J. C. Vardaxoglou, "Modelling of dynamic on-body channels using different types of wearable antennas," *The 8th European Conference on Antennas and Propagation (EuCAP 2014)*, 852–856, The Hague, 2014.
14. Lee, G., B. Garner, and Y. Li, "Investigation of on-body wave propagations using an arm-swinging phantom model and motion capture technique," *IEEE Transactions on Antennas and Propagation*, Vol. 69, No. 2, 1219–1223, February 2021.
15. Advanced MRI, National Institutes of Health, Dielectric Phantom Recipe Generator, Accessed: December 14, 2018, [Online], Available: https://amri.ninds.nih.gov/cgi-bin/phantomrecipe.
16. Federal Communications Commission, Body Tissue Dielectric Parameters, Accessed: December 14, 2018, [Online], Available: https://www.fcc.gov/general/body-tissue-dielectric-parameters.
17. Nie, Z., J. Ma, Z. Li, H. Chen, and L. Wang, "Dynamic propagation channel characterization and modeling for human body communication," *Sensors*, Vol. 12, 17569–17587, 2012.
18. Cotton, S. L., S. K. Yoo, and W. G. Scanlon, "A measurements based comparison of new and classical models used to characterize fading in body area networks," *2014 IEEE MTT-S International Microwave Workshop Series on RF and Wireless Technologies for Biomedical and Healthcare Applications (IMWS-Bio2014)*, December 2014.
19. Rosini, R., R. Verdone, and R. D'Errico, "Body-to-body indoor channel modeling at 2.45 GHz," *IEEE Transactions on Antennas and Propagation*, Vol. 62, No. 11, November 2014.
20. Bhargav, N., S. L. Cotton, G. A. Conway, A. McKernan, and W. G. Scanlon, "Simultaneous channel measurements of the on-body and body-to-body channels," *2016 IEEE 27th Annual International Symposium on Personal, Indoor, and Mobile Radio Communications (PIMRC)*, September 2016.